

# Pushing the Envelope of LLM Inference on AI-PC

Evangelos Georganas, Dhiraj Kalamkar, Alexander Heinecke  
Intel Corporation

**Abstract**—The advent of ultra-low-bit LLM models (1/1.58/2-bit), which match the perplexity and end-task performance of their full-precision counterparts using the same model size, is ushering in a new era of LLM inference for resource-constrained environments such as edge devices and AI PCs. While these quantization advances promise models that are more cost-effective in terms of latency, memory, throughput, and energy consumption, the computational efficiency of state-of-the-art (SOTA) inference runtimes (e.g., bitnet.cpp) used to deploy them remains underexplored. In this work, we take a bottom-up approach: we first design and implement 1-bit and 2-bit microkernels optimized for modern CPUs, achieving peak computational efficiency across a variety of CPU platforms. We integrate these microkernels into a state-of-the-art LLM inference framework, namely PyTorch-TPP, and present end-to-end inference results with 2-bit models that outperform the current SOTA runtime bitnet.cpp by up to 2.2 $\times$ , and deliver up to 7 $\times$  speedup compared to the 16-bit model inference. Our optimized runtime advances the state of LLM inference on AI PCs and edge devices, paving the way for efficient deployment of ultra-low-bit LLM models.

## I. INTRODUCTION

Recent advances in Quantization-Aware Training (QAT) LLM methods have produced ultra-low bit (1-bit, 1.58-bit and 2-bit) quantized models that match the perplexity and end-task performance of their full-precision counterparts using the same model size [1], [2]. Despite these advancements that yield ultra-low bit LLM models with the *potential* to be cost-effective in terms of latency, memory, throughput, and energy consumption, the available runtimes capable of serving inference with such models are limited. For example, the state-of-the-art inference runtime bitnet.cpp is specifically designed for ternary LLMs, with a relatively narrow range of applicable model architectures [3]. Additionally, although the bitnet.cpp runtime improves upon alternatives (e.g. llama.cpp) being up to 6 $\times$  faster by introducing a specialized mixed-precision matrix multiplication (mpGEMM) library to facilitate sub-2-bits model inference, its efficiency is not evaluated in terms of optimality or roofline performance. Our preliminary performance analysis showed that 2-bit inference with bitnet.cpp was even *slower* than state-of-the-art 4-bit inference on CPUs (e.g. see in Figures 9, 8, 10 the orange and the magenta bars), highlighting that the bitnet.cpp runtime is far from optimal.

In this work we adopt a bottom-up approach to address the performance shortcomings of bitnet.cpp. The key observation is that client/edge inference typically involves single-batch use-cases, which in turn result in memory-bound matrix multiplication invocations (more precisely matrix-vector multiplication) during the execution. By exploiting the reduced bit-width of the model’s weight tensors during in-

ference we can accelerate the corresponding matrix-vector multiplications (e.g. compared to the case with 16-bit weight tensors), since the volume of data read on the critical path is proportional to the bit-width of the weight datatype. First, we designed and implemented 1-bit and 2-bit mixed-precision matrix multiplication (GEMM) routines that up-convert the low-precision weight matrices (1- or 2-bit entries) to 8-bit integers, and perform the fused-multiply-add (FMA) operations using hardware-accelerated instructions on modern CPUs. We introduce novel weight layouts that facilitate the up-convert process, and within the GEMM microkernels we deploy instruction sequences that maximize the throughput of the “up-convert and compute” steps. We also construct performance models for the introduced kernels to assess their efficacy and show that they achieve close to peak roofline performance on modern CPU platforms. Furthermore, we compose these microkernels into optimized multi-threaded GEMM routines that leverage dynamic task scheduling to fully exploit the heterogeneous architectures with *performance* and *efficiency* cores. We benchmark these multi-threaded GEMM routines on a variety of modern x86 CPU platforms. Finally, we integrate these ultra-low bit GEMM routines in a SOTA inference framework, namely PyTorch TPP [4], and showcase end-to-end inference results using 2-bit and 1-bit models. Our optimized 2-bit inference is up to 7 $\times$  faster than the 16-bit inference, and outperforms bitnet.cpp by up to 2.2 $\times$ .

The contributions of this work are:

- We designed and implemented 1-bit and 2-bit GEMM kernels tailored for CPUs with AVX2 ISA. These kernels leverage novel blocked and interleaved weight tensor layouts to facilitate the up-convert process during inference. We devised performance models that characterize the effectiveness and limitations of these kernels.
- We composed these new microkernels into multi-threaded GEMM routines targeting hybrid-core architectures. We benchmarked the new routines on a set of matrices and platforms, showing that they can achieve the attainable memory bandwidth, effectively accelerating the bandwidth-bound matrix-vector multiplication operations proportionally to the bit-width of the weight’s datatypes.
- We integrated these ultra-low bit GEMM kernels in our SOTA end-to-end inference pipeline, assessed its performance on a range of models and platforms, and observed speedups up to 7 $\times$  over the 16-bit inference.
- We benchmarked our runtime against bitnet.cpp and show that our proposed solution is up to 2.2 $\times$  faster. Finally, we compare our CPU performance with the optimized

GPU 2-bit inference within `bitnet.cpp`, which includes kernels specifically tailored for the A100 platform. Our performance on contemporary x86 AI-PC CPUs is within  $2.3 \times$ – $3 \times$  of the A100 GPU, which has  $17 \times$ – $20 \times$  more bandwidth than the CPU platforms. Thus, our work pushed the envelope of LLM inference on AI-PCs and demonstrates that ultra-low-bit inference on CPUs can approach GPU-level performance.

## II. RELATED WORK

### A. LLM Inference and ultra-low bit Quantization

In recent years, several methods have been developed by academia and industry to reduce LLM inference costs [5], minimize latency and increase efficiency, including sparsification/pruning [6], knowledge distillation [7], [8] and quantization [9]–[11]. Among these, quantization reduces the precision of model weights (e.g. from 16-bits to 4-bits/2-bits/1-bit), thereby lowering memory requirements and potentially accelerating inference, especially when the target hardware supports specialized instructions or when the pipeline operates in a bandwidth-bound regime [12]. Quantization methods for LLMs generally fall into two categories: Quantization-Aware Training (QAT) and Post-Training Quantization (PTQ). QAT incorporates reduced-precision weights directly into the model’s pretraining or fine-tuning process. By accounting for quantization effects during training, QAT enables the model to adjust its parameters with awareness of limited precision, resulting in better accuracy during quantized inference. In contrast, PTQ applies quantization to a pretrained model without additional training or fine-tuning. Although QAT typically achieves higher accuracy, it is more computationally intensive and requires access to representative training datasets [2].

As LLMs continue to scale in size and training data, increasing attention has been drawn to scaling laws that balance model size and dataset size to optimize performance and computational efficiency [13]–[15]. In parallel, the field is moving towards ultra-low-bit LLMs, motivated by the significant gains in memory and compute efficiency [1], [2], [16]. This trend calls for a re-evaluation of scaling laws to consider the impact of quantization on model performance. Recent work shows that 1.58-bit (ternary) and 2-bit quantization deliver performance comparable to full-precision models in the size–accuracy trade-off, and generally outperform both 4-bit and binary quantization [2].

### B. Accelerating ultra-low-bit LLM Inference

Despite the promising results of ultra-low-bit LLMs, practical inference on edge devices remains a challenge. Recent work, such as `Bitnet.cpp` [3], introduced an inference engine tailored for BitNet b1.58b [1] and ternary LLMs. `Bitnet.cpp` includes a custom GEMM library designed for efficient, lossless inference with sub 2-bits per weight. While `Bitnet.cpp` improves upon existing frameworks like `llama.cpp` [17] (achieving up to  $6 \times$  speedup thanks to a specialized mixed-precision matrix multiplication kernel), its efficiency has not been assessed in terms of optimality or roofline performance.

Our preliminary analysis found that 2-bit inference with `Bitnet.cpp` was *slower* than state-of-the-art 4-bit inference on CPUs with PyTorch-TPP [18]. Prior research has explored primarily lookup-table (LUT)-based mixed-precision GEMMs in deep learning [19]–[22], especially for ultra-low bit-widths. In contrast, our work demonstrates that Fused Multiply-Add (FMA)-based approaches, when paired with well-designed microkernels, can achieve near-roofline performance and push the envelope of LLM inference on edge devices.

## III. ULTRA LOW-BIT GEMM MICROKERNELS

### A. Overview and background

In this section we detail the ultra-low bit GEMM microkernels, that take as input an 1-bit (int1) or 2-bit (int2) weight tensor, multiply it with the input activation tensor and produce the output activations. We refer to this technique as “up-convert and compute”. We focus on modern CPUs with AVX2 instructions that can be found on contemporary AI-PC devices. As described in Section I, we target the use-cases where the GEMMs illustrate algorithmically very low arithmetic intensity and are typically bandwidth-bound (i.e. single-batch inference). We implemented all the GEMM microkernels using the `libxsmm` library, a Just-In-Time (JIT) GEMM library that delivers SOTA GEMM performance on CPUs [4], [23]. Last but not least, our multi-threaded GEMMs use these JIT-ed microkernels as building blocks, and for parallelization we leverage `PARLOOPPER` and its hybrid scheduling capabilities to fully utilize all performance and efficiency cores [18].

### B. Interleaved Tensor Layout for 2-bit Weights

Reading 2-bit weights from memory, performing the required multiplications/additions (FMAs), and reaching bandwidth limits is challenging. Naively up-converting the int2 weights to FP32 values (e.g., via look-up tables or permutes) and then multiplying with the input activations requires an excessive number of operations, which diminishes the performance benefits of reading the low-bit data type. CPUs on modern AI PC platforms have a limited number of cores (e.g., 10–20), yet offer bandwidth on the order of 100 GB/s. As a result, the available bandwidth per core is quite high, meaning that simple FP32 FMA throughput is insufficient to saturate the per-core memory bandwidth – especially considering that we read  $8 \times$  less data than the BF16-equivalent GEMMs while performing the same number of compute operation. This negates the benefits of using the lower-bit datatype.

To address this, we quantize the input activations to int8, allowing us to leverage the int8 VNNI FMAs available on modern AVX2 CPUs. These int8 VNNI FMAs offer  $4 \times$  the throughput of FP32 FMAs. The int8 VNNI FMA requires the input vector operands to pack together four 8-bit int8 values from the logical contraction dimension of the GEMM (which we denote as  $K$  throughout the rest of the paper), and this is the so-called VNNI4 layout. Naively packing together four 2-bit values in the innermost dimension of the weight tensor to effectively form a VNNI4 layout, requires during runtime an excessive number of shifts and shuffles to (i) unpack the

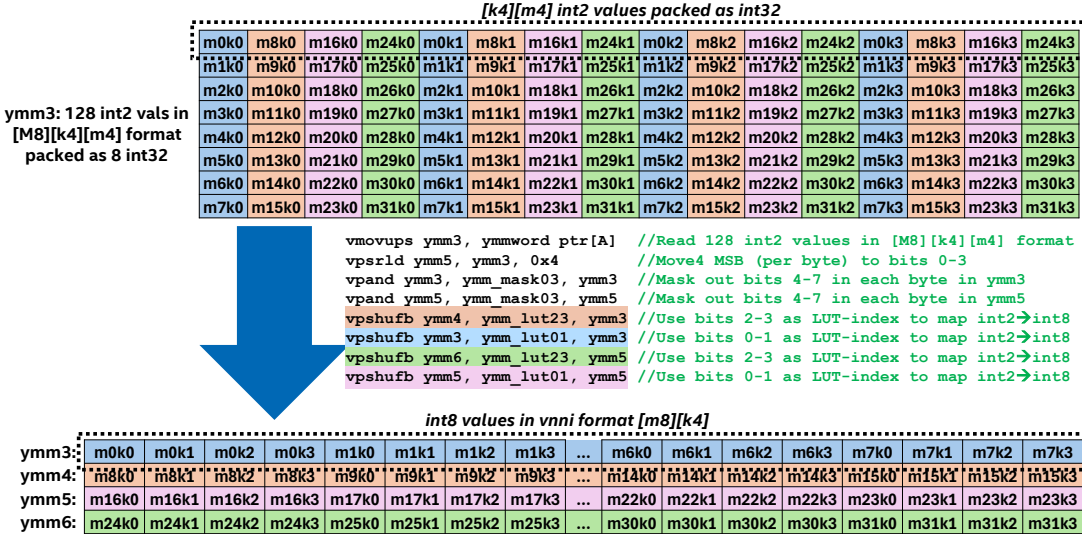


Fig. 1: Unpacking the int2 VNNI4-interleaved format to int8 VNNI4. We pack a  $[k4][m4]$  2-bit subtensor in a 32-bit value (see dotted sub-tensor in top) and with a full vector load of 256-bits we can read 128 2-bit entries, which effectively form an  $[M8][k4][m4]$  tensor. With 1 logical shift + 2 logical AND + 4 byte-shuffles we get as output 4 256-bit vectors, each holding an  $[m8][k4]$  int8 subtensor which is in VNNI4 layout.

int2 values to int8, and (ii) to re-pack the int8 values back to VNNI4 layout (with a two-level shuffle network) for the upcoming int8-VNNI FMAs.

To alleviate this unpacking bottleneck in the case of 2-bit weights, we introduce a new tensor layout called VNNI4-interleaved, illustrated in Figure 1. In this layout, a logical  $M \times K = m32 \times k4$  tensor is transformed into an interleaved 3D tensor by folding in the innermost dimension entries from the logical  $M$  dimension that are iso-modulo 8. The new tensor layout reflects a 3D tensor  $M8 \times k4 \times m4$  whereas the innermost folded  $m4$  dimension corresponds to the originally-indexed  $m32$  entries with the same modulo 8 index. In this way, we pack a  $[k4][m4]$  2-bit subtensor in a 32-bit value (see dotted sub-tensor in top of Figure 1), and with a 256-bit vector-load we can read 128 2-bit entries, which effectively form an  $[M8][k4][m4]$  tensor.

Using this layout we can simply perform table-lookups that utilize the 2-bit entries as indices and translate them to int8 values that effectively form within a 256-bit vector an  $[m8][k4]$  int8 subtensor in VNNI4 format. This int8 vector can be readily used as input to int8 VNNI FMA. In the example of unpack instruction sequence (next to blue arrow in Figure 1), with the byte-shuffle highlighted in blue  $vpshufb$   $ymm3$ ,  $ymm_lut01$ ,  $ymm3$  we consider the 32 2-bit indices highlighted in blue from the original 2-bit packed vector. The  $ymm_lut01$  considers only the bits 0-1 of each byte in the vector and maps these indices to the corresponding int8 values. In an analogous way, with the byte-shuffle highlighted in orange  $vpshufb$   $ymm4$ ,  $ymm_lut23$ ,  $ymm3$  we consider the 32 2-bit indices with orange color from the original 2-bit packed vector. The  $ymm_lut23$  considers only bits 2-3 of each byte in the vector and maps these indices to the proper

int8 values. The shift instruction  $vpsrld$   $ymm5$ ,  $ymm3$ ,  $0x4$  shifts the 4 higher bits 4-7 within each byte to the 4 lower positions such that with 2 more shuffles (highlighted with green and magenta) we can unpack the corresponding int2 values to the respective int8 values. The two logical AND vector operations ( $vpand$ ) in the unpack instruction sequence merely mask out the highest 4 bits within each byte to ensure that the byte-shuffles have the desired effect. After this instruction sequence with 1 logical shift + 2 logical AND + 4 byte-shuffles we get as output 4 256-bit vectors, each holding an  $[m8][k4]$  int8 subtensor which is in VNNI4 layout.

We emphasize that the used byte permutes/shuffles are fast on modern CPU architectures since the shuffled values do not cross 128-bit lanes within a vector. Also, the input int2 tensor is packed in this interleaved format off-line since during inference the weight tensors are “frozen” and we can freely pack/reformat them ahead of time. Even though in this section we described how we reformat a logical  $32 \times 4$  2-bit vector to a  $[M8][k4][m4]$  layout, for the entire weight tensor we adopt a blocked layout. The input weight tensor  $W$  is conceptually a 2D matrix  $W^{M \times K}$ . We follow the approach of previous work [24] and we block the dimensions  $M$ ,  $K$ , by factors  $b_m = 32$ , and  $b_k$  respectively. Such a blocked layout is exposing better locality and avoids large, strided sub-tensor accesses which are known to cause TLB misses and cache conflict misses in case the leading dimensions are large powers of 2 [24]. By using these blocking factors  $b_m = 32$ , and  $b_k$ , the logical  $[K][M]$  weight tensor is blocked and interleaved in a  $[M/32][K/b_k][b_k/4][M8][k4][m4]$  layout. We leverage the BRGEMM TPP in order to perform the tensor contraction over dimensions  $K/b_k$  and  $b_k$ , which constitute the inner-product dimension of the original 2D matrix [24].

```

vmovups ymm3, ymmword ptr[A] //Read 128 int2 values in [M8][k4][m4] format
vpsrld ymm5, ymm3, 0x4 //Move4 MSB (per byte) to bits 0-3
vpand ymm3, ymm_mask03, ymm3 //Mask out bits 4-7 in each byte in ymm3
vpand ymm5, ymm_mask03, ymm5 //Mask out bits 4-7 in each byte in ymm5
vpshufb ymm4, ymm_lut23, ymm3 //Use bits 2-3 as LUT-index to map int2→int8
vpshufb ymm3, ymm_lut01, ymm3 //Use bits 0-1 as LUT-index to map int2→int8
vpshufb ymm6, ymm_lut23, ymm5 //Use bits 2-3 as LUT-index to map int2→int8
vpshufb ymm5, ymm_lut01, ymm5 //Use bits 0-1 as LUT-index to map int2→int8
vpbroadcastd ymm7,dword ptr[B] //Broadcast 4-k int8 B values
vpdpbssd ymm12, ymm7, ymm3 //Perform int8 VNNI-FMA
vpdpbssd ymm13, ymm7, ymm4 //Perform int8 VNNI-FMA
vpdpbssd ymm14, ymm7, ymm5 //Perform int8 VNNI-FMA
vpdpbssd ymm15, ymm7, ymm6 //Perform int8 VNNI-FMA
vpbroadcastd ymm3,dword ptr[A] //Read 32 int1 values in [m8][k4] format
vpshufb ymm3, ymm3, ymm_perm //Move to i-th byte the one with the i-th bit
vpand ymm3, ymm1, ymm3 //Isolate respective i-th bit within each byte
vpcmpqeb ymm3, ymm1, ymm3 //Create mask based on 0/1 value of i-th bit
vpblendvb ymm3, ymm2, ymm3, ymm3 //Blend -1/+1 values based on mask above
vpbroadcastd ymm4,dword ptr[A+0x4] //Repeat for next 32 int1 values
vpshufb ymm4, ymm4, ymm0
vpand ymm4, ymm1, ymm4
vpcmpqeb ymm4, ymm1, ymm4
vpblendvb ymm4, ymm2, ymm4, ymm4
vpbroadcastd ymm5,dword ptr[A+0x8] //Repeat for next 32 int1 values
vpshufb ymm5, ymm5, ymm0
vpand ymm5, ymm1, ymm5
vpcmpqeb ymm5, ymm1, ymm5
vpblendvb ymm5, ymm2, ymm5, ymm5
vpbroadcastd ymm6,dword ptr[A+0xc] //Repeat for next 32 int1 values
vpshufb ymm6, ymm6, ymm0
vpand ymm6, ymm1, ymm6
vpcmpqeb ymm6, ymm1, ymm6
vpblendvb ymm6, ymm2, ymm6, ymm6
vpbroadcastd ymm7,dword ptr[B] //Broadcast 4-k int8 B values
vpdpbssd ymm12, ymm3, ymm7 //Perform int8 VNNI-FMA
vpdpbssd ymm13, ymm4, ymm7 //Perform int8 VNNI-FMA
vpdpbssd ymm14, ymm5, ymm7 //Perform int8 VNNI-FMA
vpdpbssd ymm15, ymm6, ymm7 //Perform int8 VNNI-FMA

```

Fig. 2: AVX2 GEMM microkernel with int2 weights (matrix  $A^{M \times K}$ ), int8 activations (matrix  $B^{N \times K}$ ) and vnni-INT8 FMAs ( $M = 32$ ,  $N = 1$ ,  $K = 4$ ). Matrix  $A$  uses the VNNI4-interleaved layout  $[M8][k4][m4]$  described in Section III-B.

### C. 2-bit GEMM microkernel

By leveraging the interleaved format described in section III-B we can design a mixed precision GEMM microkernel that uses 2-bit weights, 8-bit activations and produces 32-bit outputs (see Figure 2). First, with a full 256-bit vector load we load 128 int2 values in  $[M8][k4][m4]$  layout in vector register ymm3. Then with the up-convert sequence described in the previous section we unpack these 128 int2 values to 128 int8 values occupying 4 vector registers ymm3 - ymm6. With a 32-bit broadcast vpbroadcastd we broadcast in ymm7 four 8-bit values from the input activations that correspond to 4 elements from the logical  $K$  dimension that should be contracted. Finally, with four vnni-int8 FMAs (vpdpbssd) we perform the corresponding multiply-add operations among vectors ymm3 - ymm6 and vector ymm7 and we accumulate the partial products in the output 32-bit accumulators ymm12 - ymm15. This microkernel effectively multiplies a logical  $32 \times 4$   $A$  subtensor with a  $4 \times 1$   $B$  vector and produces an output  $32 \times 1$  with 32-bit integer precision. Using this microkernel as a building block, we can compose GEMM and BRGEMM microkernels with larger  $M$ ,  $K$  and  $N$  values [23], [24].

### D. 1-bit GEMM microkernel

For the 1-bit GEMM microkernel we use a conventional VNNI4 layout, where 32 int1 values are packed in an  $[m8][k4]$  subtensor. Figure 3 illustrates a microkernel that multiplies 1-bit matrix  $A$  in VNNI4 fromat with size  $32 \times 4$  with an 8-bit  $4 \times 1$  vector  $B$ . First with a 32-bit broadcast vpbroadcastd ymm3, dword ptr[A] we broadcast a logical  $[m8][k4]$  subtensor of  $A$  to within each 32-bit chunk of vector ymm3. With an in-lane byte shuffle vpshufb ymm3, ymm3, ymm\_perm we move the byte containing the  $i$ -th bit of the loaded 32-bits to the  $i$ -th byte within the 256-bit vector ymm3. Then with a logical AND operation vpand ymm3, ymm1, ymm3 we isolate within each byte the bit residing in the  $i$ -th position. After this step, we use a compare instruction vpcmpqeb ymm3, ymm1, ymm3 to use the previous isolated bits and generate a mask with byte values 0x00 or 0xff depending on the isolated values of the bits. Last, by using the generated mask we blend with the instruction vpblendvb ymm3, ymm2, ymm3, ymm3 the int8 values +1/-1 to the expanded vector ymm3. With such an instruction sequence we upconvert the logical  $[m8][k4]$  1-bit

```

vpbroadcastd ymm3,dword ptr[A] //Read 32 int1 values in [m8][k4] format
vpshufb ymm3, ymm3, ymm_perm //Move to i-th byte the one with the i-th bit
vpand ymm3, ymm1, ymm3 //Isolate respective i-th bit within each byte
vpcmpqeb ymm3, ymm1, ymm3 //Create mask based on 0/1 value of i-th bit
vpblendvb ymm3, ymm2, ymm3, ymm3 //Blend -1/+1 values based on mask above
vpbroadcastd ymm4,dword ptr[A+0x4] //Repeat for next 32 int1 values
vpshufb ymm4, ymm4, ymm0
vpand ymm4, ymm1, ymm4
vpcmpqeb ymm4, ymm1, ymm4
vpblendvb ymm4, ymm2, ymm4, ymm4
vpbroadcastd ymm5,dword ptr[A+0x8] //Repeat for next 32 int1 values
vpshufb ymm5, ymm5, ymm0
vpand ymm5, ymm1, ymm5
vpcmpqeb ymm5, ymm1, ymm5
vpblendvb ymm5, ymm2, ymm5, ymm5
vpbroadcastd ymm6,dword ptr[A+0xc] //Repeat for next 32 int1 values
vpshufb ymm6, ymm6, ymm0
vpand ymm6, ymm1, ymm6
vpcmpqeb ymm6, ymm1, ymm6
vpblendvb ymm6, ymm2, ymm6, ymm6
vpbroadcastd ymm7,dword ptr[B] //Broadcast 4-k int8 B values
vpdpbssd ymm12, ymm3, ymm7 //Perform int8 VNNI-FMA
vpdpbssd ymm13, ymm4, ymm7 //Perform int8 VNNI-FMA
vpdpbssd ymm14, ymm5, ymm7 //Perform int8 VNNI-FMA
vpdpbssd ymm15, ymm6, ymm7 //Perform int8 VNNI-FMA

```

Fig. 3: AVX2 GEMM microkernel with int1 weights and vnni-INT8 FMAs ( $M = 32$ ,  $N = 1$ ,  $K = 4$ ). Matrix  $A$  uses conventional VNNI4 layout  $[m8][k4]$ .

subtensor of  $A$  to an  $[m8][k4]$  8-bit subtensor in ymm3 that has the value +1 if the original bit in  $A$  is 0 and the value -1 if the original bit in  $A$  is 1 (this is the desired weight encoding in our 1-bit weights [2]). With a 32-bit broadcast vpbroadcastd we broadcast in ymm7 four 8-bit values from the input activations  $B$  that correspond to 4 elements from the logical  $K$  dimension that should be contracted. Finally, with a vnni-int8 FMAs (vpdpbssd ymm12, ymm3, ymm7) we perform the corresponding multiply-add operations among vectors ymm3 and vector ymm7 and we accumulate the partial product in the output 32-bit accumulator ymm12. We repeat the same up-convert and FMA sequence for the rest 96 entries of matrix  $A$  (where we reuse the input vector  $B$ ) and we conclude the int1 GEMM microkernel. With this microkernel as a building block, we compose GEMM and BRGEMM microkernels with larger  $M$ ,  $K$  and  $N$  values [24].

### E. Performance modeling

In this section we devise roofline models for the 2-bit and 1-bit GEMM microkernels to assess their efficacy and limitations. These models will be used to explain the obtained performance results in section IV. Specifically, we aim to determine under which conditions our microkernels can saturate the available bandwidth on the platform and effectively accelerate matrix-vector multiplications during inference. For our analysis we follow the reasoning/bottleneck-style analysis of the original roofline model [25]. Let  $\beta$  denote the number of bytes/cycle each core in a multi-core CPU can read when all cores access memory simultaneously. Let  $\gamma$  represent the number of cycles to *compute* an output 256-bit vector in the GEMM without considering the data load instructions. Assuming  $B$  bytes must be read from memory in order to compute an output 256-bit vector, the number of cycles  $T$  to calculate such an output 256-bit vector is:

$$T = \max(B/\beta, \gamma) \quad (1)$$

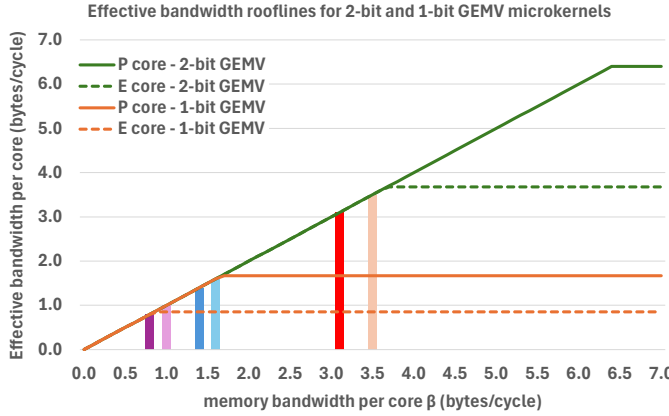


Fig. 4: Effective bandwidth rooflines for 2-bit and 1-bit GEMV microkernels considering  $P$  and  $E$  cores.

To operate in a bandwidth-bound regime, since we are reading the weight tensor from memory and the matrix-vector multiplication has no weight re-use, we need the first term in the max operator above to be the dominant one, i.e.:

$$\gamma \leq B/\beta \Rightarrow \beta \leq B/\gamma \quad (2)$$

With this annotation, we can determine the effective bandwidth per core  $e_{bw}$  to be bounded by the minimum of the terms  $\beta$  and  $B/\gamma$  (the latter term representing the throughput of the up-convert & compute sequence). In short we can write:

$$e_{bw} = \min(\beta, B/\gamma) \quad (3)$$

Since our CPU platforms have performance  $P$  and efficiency  $E$  cores with different compute capabilities, we consider two different  $\gamma$  factors, namely  $\gamma_P$  and  $\gamma_E$ , and consequently two different effective bandwidth terms  $e_{bw}^P = \min(\beta, B/\gamma_P)$  and  $e_{bw}^E = \min(\beta, B/\gamma_E)$ . For the 2-bit GEMM microkernel, the  $\gamma$  factor entails the cycles to perform (1 logical shift + 2 logical AND + 4 byte-shuffles + 4 int8 FMAs) / 4. In an analogous fashion, for the 1-bit GEMM microkernel, the  $\gamma$  factor entails the cycles to perform (1 byte-shuffle + 1 logical AND + 1 byte-compare + 1 byte-blend + 1 int8 FMA). In either case, we are interested in the throughput of these instruction sequences given the underlying dependencies, and we determined these  $\gamma$  values empirically for both  $P$  and  $E$  cores on contemporary x86 client CPUs.

Through micro-benchmarks we find that for the 2-bit kernel  $\gamma_P = 1.25$  and  $\gamma_E = 2.175$ . By setting these values in equation 3 and setting  $B = 8$  since we need to read 8 bytes to calculate an output 256-bit vector, we obtain:  $e_{bw}^P = \min(\beta, 6.4)$  and  $e_{bw}^E = \min(\beta, 3.68)$ . Figure 4 illustrates the derived rooflines for the effective bandwidth per core in bytes/cycle (y-axis) whereas the x-axis shows the available memory bandwidth per core  $\beta$  in bytes/cycle. The solid green line depicts  $e_{bw}^P$  for the 2-bit microkernel whereas the dashed green line corresponds to the  $e_{bw}^E$  for the 2-bit microkernel.

Similarly, for the 1-bit kernels we measured  $\gamma_P = 2.4$  and  $\gamma_E = 4.71$ . By setting these values in equation 3 and setting

$B = 4$  since we need to read 4 bytes to calculate an output 256-bit vector in the 1-bit case, we obtain:  $e_{bw}^P = \min(\beta, 1.7)$  and  $e_{bw}^E = \min(\beta, 0.85)$ . Figure 4 also illustrates the corresponding  $e_{bw}^P$  for the 1-bit microkernel (solid orange line) and  $e_{bw}^E$  (dashed orange line). In the next section we use this roofline performance model to analyze the efficacy of our microkernels on our CPU platforms which exhibit  $\beta$  values annotated with vertical bars in Figure 4.

## IV. RESULTS

### A. Experimental Platforms

For our evaluation we use three contemporary x86 CPUs with varying number of performance and efficiency cores, and different memory bandwidth:

- Intel Core Ultra 9 285K CPU (henceforth referred to as ARL) with 24 cores (8 performance and 16 efficiency cores). It features overclocked memory DDR5@7200 MT/s with measured read bandwidth of 98 GB/s and a Maximum Turbo Power of 250W.
- Intel Core Ultra 7 255H CPU (henceforth referred to as ARLH) with 14 cores (6 performance and 8 efficiency cores). It has memory DDR5@5600 MT/s with measured read bandwidth of 75 GB/s and Maximum Turbo Power of 115W.
- Intel Core Ultra 7 258V CPU (henceforth referred to as LNL) with 8 cores (4 performance and 4 efficiency cores). It has memory DDR5@8533 MT/s with measured read bandwidth of 97 GB/s and Maximum Turbo Power of 37W.

### B. GEMV microbenchmarks

In this Section we assess the efficacy of the ultra-low bit GEMV kernels on the aforementioned CPU platforms. For the evaluation, we extracted the weight-matrix shapes from three models: Falcon3-1B [26] model (blue plot areas), MobileLLM-1.5B [27] model (magenta plot areas) and Llama3-8B model [28] (green plot areas). These matrix shapes ( $M \times K$ ) are shown in the x-axis of Figures 5, 6 and 7. The y-axis corresponds to the attained bandwidth (in GB/s) for the corresponding matrix-vector multiplication routines (GEMV), and we show for each matrix shape three bars: i) With dark blue bar we depict the kernels with 8-bit (int8) weights, ii) with orange bars we illustrate the kernels with 2-bit (int2) weights, and iii) with green bars we show the kernels with 1-bit (int1) weights.

In Figure 5 we illustrate the GEMV micro-benchmark results on ARL. As a baseline we consider the int8 GEMM performance where essentially there is no upconvert overhead, and the GEMV microkernel merely consists of vector loads and vnni-int8 FMAs. The int2 GEMV kernels are within 10-20% of the int8 roofline and achieve bandwidth close to the machine's peak. Especially for larger matrix sizes (right side of the plot), where the OpenMP and barrier overheads are less significant, the int2 GEMV achieves bandwidth within 2-5% of the int8 GEMV. For the smallest matrix shape  $1600 \times 1600$ , given the peak read bandwidth (98 Gb/s), the ideal pure int2

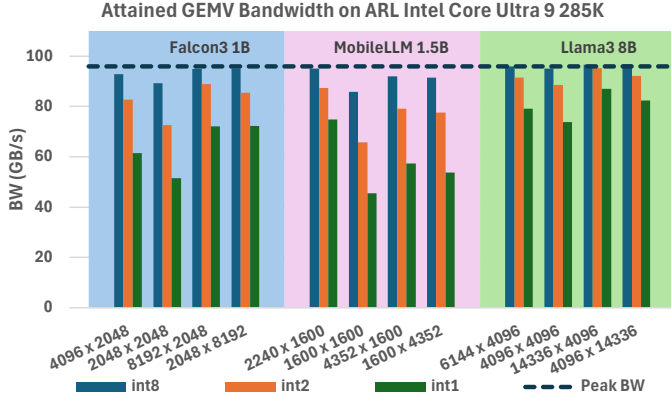


Fig. 5: Attained GEMV bandwidth on ARL for various matrix shapes and precisions (int/int2/int1).

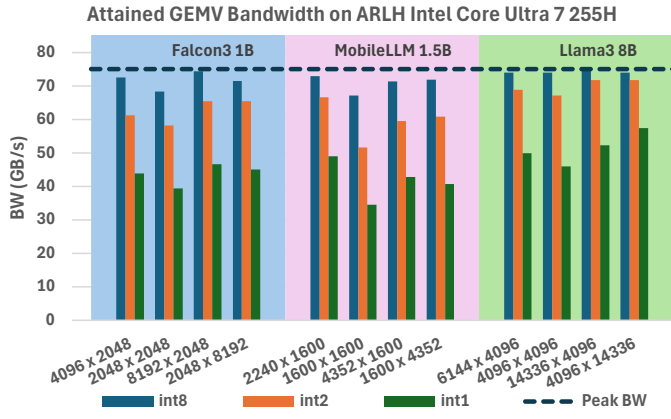


Fig. 6: Attained GEMV bandwidth on ARLH for various matrix shapes and precisions (int/int2/int1).

microkernel time is 6 microseconds, while we measure 8.9 microseconds. However, OpenMP parallel region fork/join and barrier overheads account for 1 microsecond as measured via benchmarking on ARL. In contrast, the int8 GEMV kernels move 4× more data than the int2 ones, making the relative OpenMP overhead less impactful. These overheads are even more pronounced for 1-bit weights (dark green bars).

On ARL with total read bandwidth 98 GB/s and 24 cores, each core can draw 4 GB/s assuming equal bandwidth distribution. The operating frequencies of 5.4 Ghz for  $P$  cores and 4.5 Ghz for  $E$  cores (measured under full load) translate the per-core 4 GB/s to  $\beta_P = 0.8$  bytes/cycle per  $P$  core and  $\beta_E = 0.95$  bytes/cycle per  $E$  core (see dark magenta and light magenta vertical bars in Figure 4). According to the roofline performance model, both  $P$  and  $E$  cores with the 2-bit kernel should achieve peak bandwidth (since we are residing in the slanted parts of the roofline, see green lines), which aligns with our GEMV benchmark results. Similarly, for 1-bit kernels (orange lines),  $P$  cores operate in the slanted region, while  $E$  cores are near the knee of the dotted orange line. This suggests that 1-bit GEMV on ARL should deliver near-peak bandwidth, modulo OpenMP overheads.

Figure 6 shows GEMV results on ARLH. The conclusions are similar to ARL: int2 GEMV kernels are within 10–20%

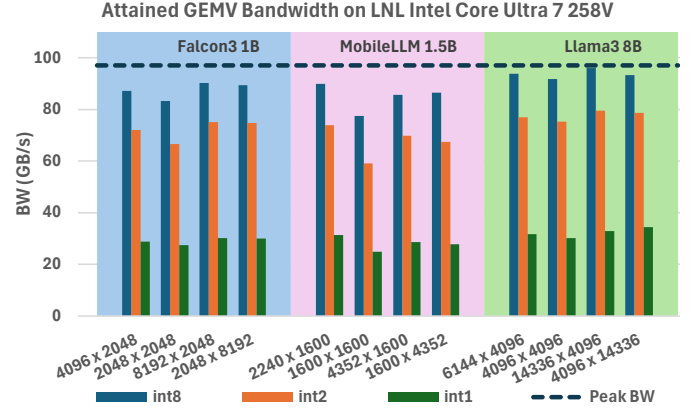


Fig. 7: Attained GEMV bandwidth on LNL for various matrix shapes and precisions (int/int2/int1).

of the int8 roofline and achieve near-peak bandwidth. With 75 GB/s total bandwidth and 14 cores, each core can draw 5.36 GB/s assuming equal bandwidth distribution. The operating frequencies of 4 GHz ( $P$  cores) and 3.6 GHz ( $E$  cores) yield  $\beta_P = 1.44$  and  $\beta_E = 1.6$  bytes/cycle (see dark and light blue vertical bars in Figure 4). For the 2-bit GEMV case, both  $P$  and  $E$  cores are modeled to hit peak bandwidth (slanted green lines), and it is confirmed by our GEMV benchmarks. For the 1-bit GEMV case,  $P$  cores saturate the available bandwidth (dark blue bar intersects slanted orange line in Figure 4), while  $E$  cores are limited by the upconvert-and-compute sequence (light blue bar intersects first flat part of dotted orange line). This means  $E$  cores on ARLH with 1-bit kernels can read up to 0.85 bytes/cycle or 2.85 GB/s. With 6  $P$  and 8  $E$  cores, the modeled bandwidth is 55 GB/s, closely matching observed values for larger matrices (dark green bars in Figure 6).

Finally, Figure 7 shows the GEMV microbenchmarks on the LNL platform. We observe that the 2-bit microkernel continues to deliver performance close to the theoretical peak (within 20–25% for the larger matrix shapes), while the 1-bit GEMV yields consistently lower performance, around 30 GB/s across all cases. On LNL, with a total read bandwidth of 97 GB/s and 8 cores, the per-core bandwidth is approximately 12.1 GB/s. The measured operating frequencies of 4.1 GHz for  $P$  cores and 3.7 GHz for  $E$  cores translate to  $\beta_P = 3.18$  bytes/cycle and  $\beta_E = 3.52$  bytes/cycle (see dark red and light red vertical bars in Figure 4). For the 2-bit GEMV kernels, we conclude that both  $P$  and  $E$  cores are able to reach close to peak read bandwidth, which is confirmed by the GEMV microbenchmark results. However, for the 1-bit GEMV kernels, both  $P$  and  $E$  cores are limited by the upconvert-and-compute sequence, as indicated by the vertical red bars intersecting first the flat regions of the solid and dotted orange rooflines. As a result, the effective bandwidth for the 1-bit kernel on LNL is limited to 6.5 GB/s per  $P$  core and 2.92 GB/s per  $E$  core, yielding a total modeled bandwidth of approximately 37 GB/s (4  $P$  + 4  $E$  cores). This explains the relatively poor performance of the 1-bit GEMV microbenchmarks on LNL. In conclusion, on LNL that offers relatively high read bandwidth and only 8 cores, the 1-bit kernels are unable to saturate the available

Next token inference throughput on ARL Intel Core Ultra 9 285K

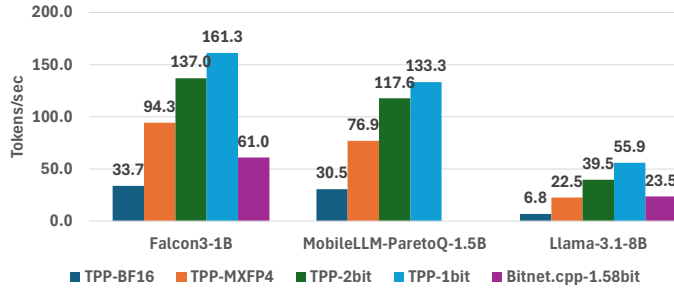


Fig. 8: End-to-end inference on ARL. For the inference with PyTorch-TPP we have four variants: (i) Dark blue bars correspond to BF16 weights. (ii) Orange bars correspond to MXFP4 weights, (iii) Green bars correspond to 2-bit weights, (iv) Light blue bars correspond to 1-bit weights. With magenta bars we represent the performance of the bitnet.cpp framework.

bandwidth. The upconvert-and-compute sequence becomes the bottleneck, limiting the overall performance of 1-bit GEMV kernels.

#### C. End to end inference results

We integrated our multi-threaded 2-bit and 1-bit GEMMs into the optimized PyTorch-TPP framework, which delivers state-of-the-art inference performance on CPUs [18]. For evaluation, we focus on three LLM models: Falcon3-1B [26], MobileLLM-1.5B [27], and Llama3-8B [28]. The MobileLLM family, released by Meta as a companion to the recent ParetoQ work, is truly quantized to 2-bit and 1-bit using QAT techniques, achieving state-of-the-art accuracy for their respective model sizes [2]. The same QAT techniques have been applied to Llama3 models, producing high-accuracy 1-bit and 2-bit variants, although the weights have not yet been released. Therefore, for performance evaluation, we use dummy 1-bit/2-bit weights for Llama3-8B. Since bitnet.cpp has limited model coverage, we include Falcon3-1B (which is supported by bitnet.cpp) as the smallest benchmarked model and also use dummy 1-bit/2-bit weights for performance runs. All experiments generate 128 output tokens with batch size 1. For bitnet.cpp, we test various core configurations and report the best result. Additionally, since PyTorch-TPP supports MXFP4 (4-bit) Weight-Only Quantization (WOQ), we benchmark this variant as well [29].

Figure 8 illustrates the end-to-end inference results on ARL. For the inference with PyTorch-TPP we have four variants: (i) Dark blue bars correspond to BF16 weights. (ii) Orange bars correspond to MXFP4 weights, (iii) Green bars correspond to 2-bit weights, (iv) Light blue bars correspond to 1-bit weights. With magenta bars we represent the performance of the bitnet.cpp framework. The measured performance is in tokens/second (y-axis). First of all, we observe that the 4-bit inference with PyTorch-TPP is faster than bitnet.cpp on the 1B parameter model and on par with bitnet.cpp for the 8B model, even though bitnet.cpp uses 2-bit weights (and as such should be substantially faster than the 4-bit inference).

Next token inference throughput on ARLH Intel Core Ultra 7 255H

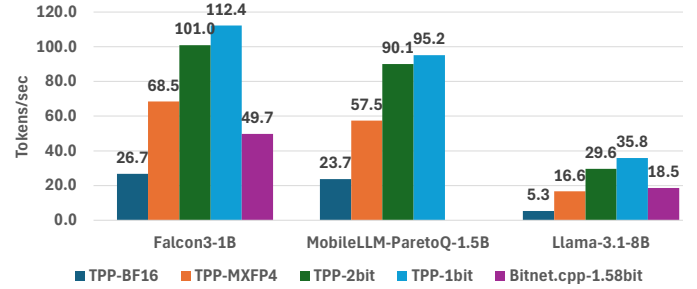


Fig. 9: End-to-end inference on ARLH.

These results suggest that bitnet.cpp is far from optimal. In our case, we observe with our optimized 2-bit inference substantial speedups over the 16-bit baseline, more precisely  $4.1\times$ ,  $3.9\times$  and  $5.8\times$  for the respective 1B, 1.5B and 8B models. With 1-bit inference we further accelerate the end-to-end pipeline over the 16-bit case by factors  $4.8\times$ ,  $4.4\times$  and  $8.3\times$  for the respective 1B, 1.5B and 8B models.

To understand these results, let us derive some performance models. More specifically, given the end-to-end inference execution we know that only the GEMV portions can be accelerated with our new kernels. Assuming that in the 16-bit inference execution the GEMV kernels constitute a fraction  $\alpha$  of the total execution time, and by applying the reasoning of Amdahl’s law, the maximum attainable speedup  $s$  over the 16-bit inference by using a datatype  $x$  times smaller is:

$$s = \frac{1}{1 - \alpha + \frac{\alpha}{x}} \quad (4)$$

For the 1B model, in the 16-bit run on ARL we get  $\alpha = 0.87$  (i.e. 87% of the time is spent in the GEMVs), and as a result the maximum attainable speedup is  $4.3\times$  for the 2-bit inference ( $x = 8$ ) and  $5.5\times$  for the 1-bit inference ( $x = 16$ ). Under this lens, we indeed see that our obtained results are close to the ideal ones (we observed  $4.1\times$  and  $4.8\times$  respectively). On the other extreme with the 8B model, in the 16-bit run we get on ARL  $\alpha = 0.96$  (i.e. 96% of the time is spent in the GEMVs), and consequently the maximum attainable speedup is  $6.1\times$  for the 2-bit inference ( $x = 8$ ) and  $9.6\times$  for the 1-bit inference ( $x = 16$ ). Again we see that our obtained results are close to the ideal ones (we observed  $5.8\times$  and  $8.3\times$  speedup over the 16-bit baseline).

When comparing our 2-bit inference with the 1.58-bit inference of bitnet.cpp we observe on ARL speedups of  $2.2\times$  for the 1B model and  $1.7\times$  for the 8B case, showing that our optimized 2-bit kernels along with the PyTorch-TPP runtime are improving substantially the SOTA 2-bit inference on CPUs.

Figure 9 exhibits the end-to-end inference results on ARLH. The high level picture is similar to the one described in the ARL case: we observe with our optimized 2-bit inference speedups over the 16-bit baseline, more precisely  $3.8\times$ ,  $3.8\times$  and  $5.6\times$  for the respective 1B, 1.5B and 8B models. With 1-bit inference we further accelerate the end-to-end pipeline over the 16-bit case by factors  $4.2\times$ ,  $4\times$  and  $6.8\times$  for the respective

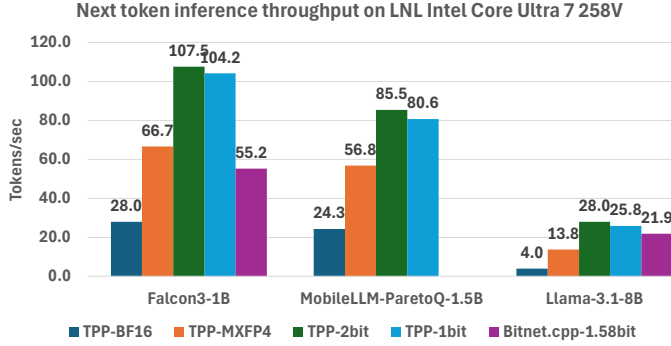


Fig. 10: End-to-end inference on LNL.

1B, 1.5B and 8B models. When comparing our 2-bit inference with the 1.58-bit inference of bitnet.cpp we observe on ARLH speedups of  $2\times$  for the 1B model and  $1.6\times$  for the 8B case.

Figure 10 depicts the end-to-end inference results on LNL. We observe with our optimized 2-bit inference speedups over the 16-bit baseline, more precisely  $3.8\times$ ,  $3.5\times$  and  $7\times$  for the respective 1B, 1.5B and 8B models. For the 1-bit case however, we are not observing any further speedups; this behavior is completely justified by the 1-bit GEMV microbenchmark results analyzed in section IV-B. On LNL with relatively high read bandwidth available and only 8 cores, the 1-bit kernels can not saturate the full available bandwidth and the upconvert & compute sequence is the bottleneck. When comparing our 2-bit inference with the 1.58-bit inference of bitnet.cpp we observe on LNL speedups of  $1.9\times$  for the 1B model and  $1.3\times$  for the 8B case.

#### D. Comparison with 2-bit inference on GPU

In a recent update, bitnet.cpp included CUDA optimized 2-bit kernels tailored for the NVIDIA A100 platform, and we were able to reproduce the reported results in that repo<sup>1</sup> on our local A100 GPU. To have an apples-to-apples comparison with our CPU results, we benchmarked our 2-bit inference pipeline on a same-size 2 Billion parameter model<sup>2</sup>. On the A100 GPU and with the bitnet-b1.58 2 Billion model we were able to obtain 250 tokens/s, whereas we achieve on the aforementioned same-sized 2B model 110 tokens/s on ARL, 82 tokens/s on ARLH, and 88 tokens/s on LNL. As a result, we conclude that this level of performance on the CPUs is within  $2.3\times$ - $3\times$  of the A100 GPU which has  $17\times$ - $20\times$  more bandwidth than our CPUs. To further shed light on these results, we assessed the efficacy of the 2-bit GEMV kernels on A100 compared to the corresponding 16-bit ones (these results are also provided in the bitnet.cpp and we were able to reproduce them). On the A100 GPU, for the smaller matrix shapes (e.g.  $2560\times 2560$ ,  $3840\times 2560$ ,  $3200\times 3200$ ) the observed 2-bit GEMV speedup over the 16-bit GEMV is only  $1.3\times$ - $1.4\times$  whereas for the larger shapes the speedup goes up to  $3.6\times$ . Considering that the majority of matrices in such LLMs (i.e. 2B) are relatively small, we expect the upside of the 2-bit GEMVs to be limited on A100. For comparison,

in similarly-sized matrices we were able to observe close to ideal bandwidth with our 2-bit GEMV kernels on CPUs, meaning that they are  $\approx 7\times$  faster than the corresponding 16-bit GEMVs, and as a result we materialized substantial speedup in the end-to-end 2-bit inference.

## V. CONCLUSIONS AND FUTURE WORK

In this work, we designed and implemented 1-bit and 2-bit GEMM microkernels optimized for modern x86 CPUs, achieving close to roof-line efficiency across a variety of CPU platforms. We integrated these microkernels into a state-of-the-art LLM inference framework and presented end-to-end inference results with 2-bit models that outperform the current SOTA runtime (bitnet.cpp) by up to  $2.2\times$ , and deliver up to  $7\times$  speedup compared to the 16-bit model inference. Our optimized runtime advances the state of LLM inference on AI PCs and edge devices, paving the way for efficient deployment of ultra-low-bit LLM models. Additionally we demonstrate that with proper microkernel design and runtime support, ultra-low-bit inference on CPUs can approach GPU-level performance. As future work we plan to extend our work to ARM platforms, since essentially our 1-bit and 2-bit microkernels can be readily translated to AArch64 and SVE instructions which are available on modern ARM CPUs.

## REFERENCES

- [1] Shuming Ma, Hongyu Wang, Lingxiao Ma, Lei Wang, Wenhui Wang, Shaohan Huang, Li Dong, Ruiping Wang, Jilong Xue, and Furu Wei. The era of 1-bit llms: All large language models are in 1.58 bits, 2024.
- [2] Zechun Liu, Changsheng Zhao, Hanxian Huang, Sijia Chen, Jing Zhang, Jiawei Zhao, Scott Roy, Lisa Jin, Yunyang Xiong, Yangyang Shi, et al. Paretoq: Scaling laws in extremely low-bit llm quantization. *arXiv preprint arXiv:2502.02631*, 2025.
- [3] Jinheng Wang, Hansong Zhou, Ting Song, Shijie Cao, Yan Xia, Ting Cao, Jianyu Wei, Shuming Ma, Hongyu Wang, and Furu Wei. Bitnet.cpp: Efficient edge inference for ternary llms, 2025.
- [4] Evangelos Georganas, Dhiraj Kalamkar, Sasikanth Avancha, Menachem Adelman, Cristina Anderson, Alexander Breuer, Jeremy Bruestle, Narendra Chaudhary, Abhisek Kundu, Denise Kutnick, et al. Tensor processing primitives: A programming abstraction for efficiency and portability in deep learning workloads. In *Proceedings of the International Conference for High Performance Computing, Networking, Storage and Analysis*, pages 1–14, 2021.
- [5] Marcos Treviso, Ji-Ung Lee, Tianchu Ji, Betty van Aken, Qingqing Cao, Manuel R Ciosici, Michael Hassid, Kenneth Heafield, Sara Hooker, Colin Raffel, et al. Efficient methods for natural language processing: A survey. *Transactions of the Association for Computational Linguistics*, 11:826–860, 2023.
- [6] Elias Frantar and Dan Alistarh. Sparsegpt: Massive language models can be accurately pruned in one-shot. In *International Conference on Machine Learning*, pages 10323–10337. PMLR, 2023.
- [7] Geoffrey Hinton, Oriol Vinyals, and Jeff Dean. Distilling the knowledge in a neural network. *arXiv preprint arXiv:1503.02531*, 2015.
- [8] Rohan Taori, Ishaan Gulrajani, Tianyi Zhang, Yann Dubois, Xuechen Li, Carlos Guestrin, Percy Liang, and Tatsunori B Hashimoto. Stanford alpaca: An instruction-following llama model, 2023.
- [9] Ji Lin, Jiaming Tang, Haotian Tang, Shang Yang, Wei-Ming Chen, Wei-Chen Wang, Guangxuan Xiao, Xingyu Dang, Chuang Gan, and Song Han. Awq: Activation-aware weight quantization for on-device llm compression and acceleration. *Proceedings of Machine Learning and Systems*, 6:87–100, 2024.
- [10] Jerry Chee, Yaohui Cai, Volodymyr Kuleshov, and Christopher M De Sa. Quip: 2-bit quantization of large language models with guarantees. *Advances in Neural Information Processing Systems*, 36:4396–4429, 2023.

<sup>1</sup><https://github.com/microsoft/BitNet/tree/main/gpu>

<sup>2</sup><https://huggingface.co/andrijdavid/Llama3-2B-Base>

- [11] Zechun Liu, Changsheng Zhao, Hanxian Huang, Sijia Chen, Jing Zhang, Jiawei Zhao, Scott Roy, Lisa Jin, Yunyang Xiong, Yangyang Shi, et al. Paretoq: Scaling laws in extremely low-bit lilm quantization. *arXiv preprint arXiv:2502.02631*, 2025.
- [12] Jiedong Lang, Zhehao Guo, and Shuyu Huang. A comprehensive study on quantization techniques for large language models. In *2024 4th International Conference on Artificial Intelligence, Robotics, and Communication (ICAIRC)*, pages 224–231. IEEE, 2024.
- [13] Jordan Hoffmann, Sébastien Borgeaud, Arthur Mensch, Elena Buchatskaya, Trevor Cai, Eliza Rutherford, Diego de Las Casas, Lisa Anne Hendricks, Johannes Welbl, Aidan Clark, et al. Training compute-optimal large language models. *arXiv preprint arXiv:2203.15556*, 2022.
- [14] Tanishq Kumar, Zachary Ankner, Benjamin F Spector, Blake Bordelon, Niklas Muenmighoff, Mansheej Paul, Cengiz Pehlevan, Christopher Ré, and Aditi Raghunathan. Scaling laws for precision. *arXiv preprint arXiv:2411.04330*, 2024.
- [15] Tim Dettmers and Luke Zettlemoyer. The case for 4-bit precision: k-bit inference scaling laws. In *International Conference on Machine Learning*, pages 7750–7774. PMLR, 2023.
- [16] Zechun Liu, Barlas Oguz, Aasish Pappu, Yangyang Shi, and Raghuraman Krishnamoorthi. Binary and ternary natural language generation. *arXiv preprint arXiv:2306.01841*, 2023.
- [17] Georgi Gerganov. llama.cpp: Llm inference in c/c++, <https://github.com/ggml-org/llama.cpp>.
- [18] Evangelos Georganas, Dhiraj Kalamkar, Kirill Voronin, Abhisek Kundu, Antonia Noack, Hans Pabst, Alexander Breuer, and Alexander Heinecke. Harnessing deep learning and hpc kernels via high-level loop and tensor abstractions on cpu architectures. In *2024 IEEE International Parallel and Distributed Processing Symposium (IPDPS)*, pages 950–963. IEEE, 2024.
- [19] Darshan C Ganji, Saad Ashfaq, Ehsan Saboori, Sudhakar Sah, Saptarshi Mitra, Mohammadhossein Askarihemmat, Alexander Hoffman, Ahmed Hassanien, and Mathieu Leonardon. Deepgemm: Accelerated ultra low-precision inference on cpu architectures using lookup tables. In *Proceedings of the IEEE/CVF conference on computer vision and pattern recognition*, pages 4656–4664, 2023.
- [20] Davis Blalock and John Guttag. Multiplying matrices without multiplying. In *International Conference on Machine Learning*, pages 992–1004. PMLR, 2021.
- [21] Xiaohu Tang, Yang Wang, Ting Cao, Li Lyna Zhang, Qi Chen, Deng Cai, Yunxin Liu, and Mao Yang. Lut-nn: Empower efficient neural network inference with centroid learning and table lookup. In *Proceedings of the 29th Annual International Conference on Mobile Computing and Networking*, pages 1–15, 2023.
- [22] Jianyu Wei, Shijie Cao, Ting Cao, Lingxiao Ma, Lei Wang, Yanyong Zhang, and Mao Yang. T-mac: Cpu renaissance via table lookup for low-bit lilm deployment on edge, 2024. URL <https://arxiv.org/abs/2407.00088>.
- [23] Alexander Heinecke, Greg Henry, Maxwell Hutchinson, and Hans Pabst. Libxsmm: accelerating small matrix multiplications by runtime code generation. In *SC'16: Proceedings of the International Conference for High Performance Computing, Networking, Storage and Analysis*, pages 981–991. IEEE, 2016.
- [24] Evangelos Georganas, Kunal Banerjee, Dhiraj Kalamkar, Sasikanth Avancha, Anand Venkat, Michael Anderson, Greg Henry, Hans Pabst, and Alexander Heinecke. Harnessing deep learning via a single building block. In *2020 IEEE International Parallel and Distributed Processing Symposium (IPDPS)*, pages 222–233. IEEE, 2020.
- [25] Samuel Williams, Andrew Waterman, and David Patterson. Roofline: an insightful visual performance model for multicore architectures. *Communications of the ACM*, 52(4):65–76, 2009.
- [26] Falcon3-1b-instruct, <https://huggingface.co/tiiuae/Falcon3-1B-Instruct>.
- [27] Mobilellm-paretoq-1.5b, <https://huggingface.co/facebook/MobileLLM-ParetoQ-1.5B-BF16>.
- [28] Llama-3.1-8b, <https://huggingface.co/meta-llama/Llama-3.1-8B>.
- [29] Evangelos Georganas, Dhiraj Kalamkar, Alexander Kozlov, and Alexander Heinecke. MI-specqd: Multi-level speculative decoding with quantized drafts. *arXiv preprint arXiv:2503.13565*, 2025.

Optimization Notice: Software and workloads used in performance tests may have been optimized for performance only on Intel microprocessors. Performance tests, such as SYSmark and MobileMark, are measured using specific computer systems, components, software, operations and functions. Any change to any of those factors may cause

the results to vary. You should consult other information and performance tests to assist you in fully evaluating your contemplated purchases, including the performance of that product when combined with other products. For more information go to <http://www.intel.com/performance>. Intel, Xeon, and Intel Xeon Phi are trademarks of Intel Corporation in the U.S. and/or other countries.

## APPENDIX

### A. Reproducing end-to-end inference with PyTorch-TPP

To install the PyTorch-TPP runtime:

```
git clone https://github.com/libxsmm/tpp-pytorch-extension.git
cd tpp-pytorch-extension
git checkout 2bit_gemm
git submodule update --init
bash utils/setup_conda.sh
source env.sh
python setup.py install
cd examples/llm/
pip install -r requirements.txt
```

In order to run the end-to-end inference experiments there is an exemplary script in examples/llm: `tpp_bakeoff_template.sh`. In this script one can define the number of  $P$  Cores (PCORES) and Total number of cores (CORES) (i.e. the number of  $E$  cores is CORES-PCORES).